ACTA IMEKO
ISSN: 2221-870X
March 2021, Volume 10, Number 1, 142 - 149

Fringe-projection profilometry for recovering 2.5D shape of ancient coins

Giuseppe Schirripa Spagnolo[1], Lorenzo Cozzella[1], Fabio Leccese[2]

[1] *Università degli Studi Roma Tre, Dipartimento di Matematica e Fisica, Rome, Italy*
[2] *Università degli Studi Roma Tre, Dipartimento di Scienze I, Rome, Italy*

ABSTRACT
The form of relief is undoubtedly one of the most topical subjects in the field of cultural heritage. Physical access to historic and artistic products can be limited by a number of factors. For example, access to collections of ancient coins is difficult, especially for students. Indeed, coin digital archives containing high-quality three-dimensional models and that can be accessed remotely are of great interest. The use of projected fringes for the measurement of surface profiles is a well-developed technique. In this paper, we present a surface-profile measurement system for small cultural heritage objects where it is important not only to detect the shape with a high degree of accuracy but also to capture and archive any signs of ageing. The equipment presented in this paper is simple, reliable and cheap. In addition, some examples are presented to demonstrate the potential of the proposed scheme for recovering 2.5D shapes of cultural heritage objects.

Section: RESEARCH PAPER

Keywords: Temporal phase unwrapping; Profilometry; Cultural heritage; 2.5D reconstruction

Citation: Giuseppe Schirripa Spagnolo, Lorenzo Cozzella, Fabio Leccese, Fringe projection profilometry for recovering 2.5D shape of ancient coins, Acta IMEKO, vol. 10, no. 1, article 19, March 2021, identifier: IMEKO-ACTA-10 (2021)-01-19

Section Editor: Carlo Carobbi, University of Florence, Italy

Received May 14, 2020; **In final form** August 5, 2020; **Published** March 2021

Corresponding author: Fabio Leccese, e-mail: fabio.leccese@uniroma3.it

1. INTRODUCTION

Given its importance in many fields, ranging from quality control to medicine, from robotics to solid modelling, surveys of surface profiles by means of non-contact optical systems is the subject of extensive studies [1]:

- In the field of cultural heritage, 3D acquisition is used primarily for documentation, comparative studies [2], [3], remote examination [4], [5] and degradation monitoring [6] as well as to create virtual museums [7, 8].
- In medicine, 3D scanners are useful for obtaining accurate anthropometric body segment parameters for the biomechanical analysis of human motion [9] and for the accurate acquisition of patient dentition [10].
- In the field of forensics, 3D reconstructions are helpful for the analysis of writing [11], [12], the virtual reconstruction of crime scenes [13], firearm examination proficiency tests [14] and face recognition [15], [16]
- In quality control, 3D scanning can be used for production control and tool wear analysis [17]-[20]. Furthermore, it can be used for underwater 3D reconstruction [21], [22].

In the field of cultural heritage conservation, both the determination of surface finish (surface texture) and its variations over time are important. In fact, in order to establish the actual vulnerability of cultural assets, one of the most important parameters to determine is the loss of material or, more generally, the determination of microstructural changes in the exposed surface (currently, for these determinations, indirect methods are used). Therefore, the objective of the present research is to develop a non-contact optoelectronic system capable of analysing, at high resolution, the surface profile of artistic finds. The basic methodology to be used for the development of the system is the one known as grating projection or structured light [23]-[25]. This method, supported by optoelectronic signal-processing techniques, allows the development of a system characterised by its high precision, small footprint and relatively low production cost.

2. THE RANGE FINDER

Projected-fringe profilometry is one of the most effective methods of measuring the 2.5D surface profiles of rough

engineering surfaces [26]-[28]. The fringe can be generated by projecting parallel light through optical grating slides with various projecting patterns, such as sinusoidal-like modulation. The traditional phase-shifting method, which involves physically moving a grating or a reference mirror, has two problems, namely, inefficiency due to mechanical movement and unavoidable phase-shifting errors incurred during the phase-shifting process. Therefore, a digital micro-mirror device has been proposed to generate flexible structured-light patterns with highly precise phase shifting.

This paper presents a surface-profile measurement method for micro-components based on the fringe-projection, phase-shifting technique and temporal phase unwrapping. Linear sinusoidal fringe patterns are projected onto an artwork surface by a digital fringe projector. The projected sinusoidal fringes will be deformed by surface height variations. By detecting the deformed sinusoidal fringes in combination with phase stepping and temporal phase unwrapping, high-precision 2.5D surface measurements can be efficiently acquired.

As shown in Figure 1, the system is a telecentric phase-shifting projected fringe profilometry tool for small objects [29]. Our tool consists of three main modules: a digital fringe projector, a charged-coupled device (CCD) camera and a computer.

Telecentric projection is realised by means of a commercially available digital light processing video projector (1920 × 1200 resolution), in which the projection lens is replaced by a telecentric lens. The optical telecentric imaging consists of a B/W CCD camera with a resolution of 1280 × 1020 and a telecentric lens. The measurement field size is about 120 mm × 100 mm and the depth of field reaches 10 mm, which is usually sufficient to measure the depth of a small, complex 3D object (i.e. an ancient coin).

The optical axis of the projector is perpendicular to the reference plane and intersects with that of the camera at the reference plane. The line connecting the exit pupil of the projector and the entrance pupil of the camera is parallel to the reference plane.

Figure 2 shows the constructed system.

Structured light with sinusoidal fringes is projected onto the object surface. Due to the depth variation of the surface, the structured light is phase modulated, leading to a deformed spatial

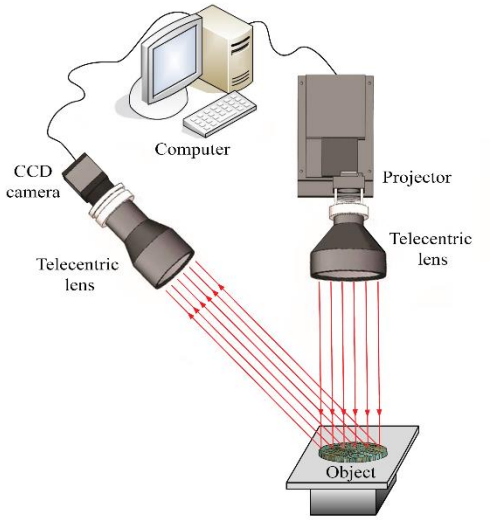

Figure 1. Basic setup for measuring surface profiles with projected fringes.

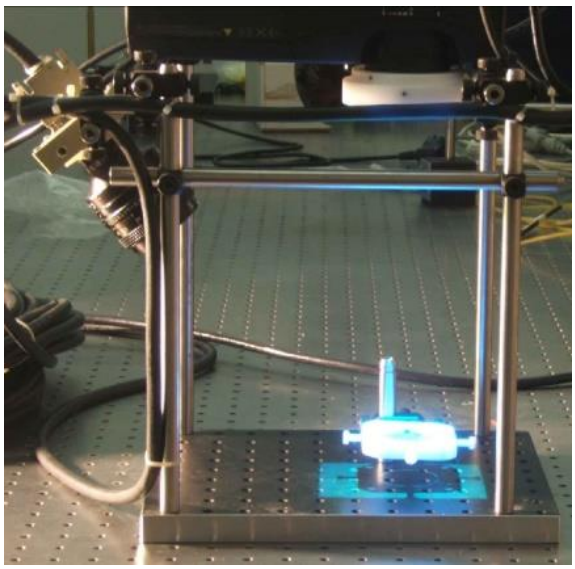

Figure 2. The layout of the fringe-projection system.

carrier fringe pattern in which the topographic information of the object surface has been encoded.

Without loss of generality, it is assumed that the fringes are in the x–y plane and perpendicular to the y-axis. The optical geometry of the phase-measuring techniques is shown in Figure 3.

The intensity distribution of the fringe-pattern image can be expressed as [30]-[33]

$$I(x,y) = I_0(x,y) + M(x,y)\cos\left[\frac{2\pi}{d}y + \varphi(x,y)\right], \quad (1)$$

where (x,y) denotes an arbitrary point in the image, $I_0(x,y)$ is the background intensity, $M(x,y)$ is the intensity modulation amplitude, $d = \frac{p_0}{cos\theta}$ is the period of the fringe seen by the CCD camera on the reference plane and $\varphi(x,y)$ is a phase change related to the 2.5D profile of the measured object. In other

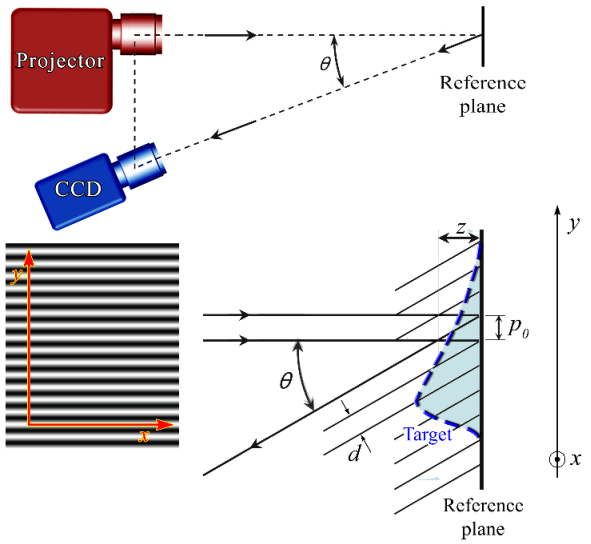

Figure 3. Optical geometry for fringe projection. In the realised system, we have θ ≈ 45°; field of view x ≈ 100 mm, y ≈ 120 mm; max z ≈ 10 mm; minimum period of projected fringe p_0 ≈ 0.5 mm; minimum period of the fringe seen by the CCD d ≈ 1.0 mm.

words, phase $\varphi(x,y)$ contains the information about the surface height/depth variations.

The relationship between the phase distribution and the profile information $z(x,y)$ of the measured object can be achieved by [34]-[37]

$$\frac{1}{z(x,y)} = a(x,y) + b(x,y)\frac{1}{\varphi(x,y)} + c(x,y)\frac{1}{\varphi^2(x,y)}, \tag{2}$$

where $a(x,y)$, $b(x,y)$ and $c(x,y)$ are the parameters related to the measurement system, which can be determined by a calibration process in advance [38]-[40].

To calculate the system constants $a(x,y)$, $b(x,y)$ and $c(x,y)$, we use the least-squares method.

As shown in Figure 4, during the calibration procedure, the reference plane is shifted to n position along the direction of the object height. Each new position has height z_n with respect to the zero position (z_0).

To determine the system constants $a(x,y)$, $b(x,y)$ and $c(x,y)$, we define the error function as

$$\varepsilon(x,y) = \sum_{n=1}^{N}\left\{\frac{1}{z(x,y)} - \left[a(x,y) + b(x,y)\cdot\frac{1}{\varphi_n(x,y)} + b(x,y)\cdot\frac{1}{\varphi_n^2(x,y)}\right]\right\}^2, \tag{3}$$

where N is the number of shifts of the standard reference plane. In the least-squares sense, the system constants $a(x,y)$, $b(x,y)$ and $c(x,y)$ can be directly estimated by minimising the sum of square $\varepsilon(x,y)$. The minimum error is at the point where the partial derivatives of $\varepsilon(x,y)$ with respect to $a(x,y)$, $b(x,y)$ and $c(x,y)$ are all zero. Therefore, we have [35]

$$\begin{bmatrix} a(x,y) \\ b(x,y) \\ c(x,y) \end{bmatrix} = \begin{bmatrix} N & \sum_1^N \frac{1}{z_n(x,y)} & \sum_1^N \frac{1}{z_n^2(x,y)} \\ \sum_1^N \frac{1}{z_n(x,y)} & \sum_1^N \frac{1}{z_n^2(x,y)} & \sum_1^N \frac{1}{z_n^3(x,y)} \\ \sum_1^N \frac{1}{z_n^2(x,y)} & \sum_1^N \frac{1}{z_n^2(x,y)} & \sum_1^N \frac{1}{z_n^4(x,y)} \end{bmatrix}^{-1} \times \begin{bmatrix} \sum_1^N \cdot \frac{1}{\varphi_n(x,y)} \\ \sum_1^N \frac{1}{z_n(x,y)} \cdot \frac{1}{\varphi_n(x,y)} \\ \sum_1^N \frac{1}{z_n^2(x,y)} \cdot \frac{1}{\varphi_n(x,y)} \end{bmatrix}. \tag{4}$$

Thus, if the phase map of N planes and the relative positions z_n are known, the system constants can be obtained from Equation 4.

For the phase calculation, it is possible to use the fast Fourier transform algorithm [41]-[43] or phase-shifting technique [23].

Generally, phase $\phi(x,y) = 2\pi\cdot\frac{y}{d} + \varphi(x,y)$ can be retrieved using the phase-shifting method. With this technique, a

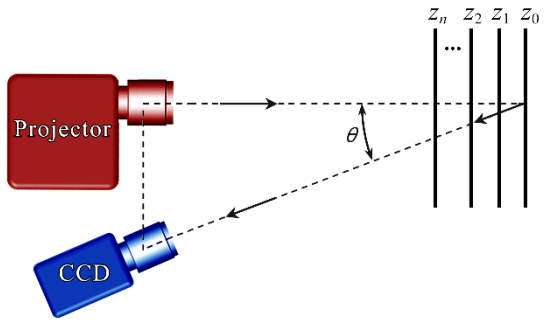

Figure 4. The calibration process of the system constant.

set of phase-shifted sinusoidal fringe patterns is projected onto the object's surface. The intensity values, captured by the CCD camera, can be expressed as [44]-[47]

$$I_n(x,y) = I_0(x,y) + M(x,y)\cos\left[\phi(x,y) + \frac{n-1}{N}2\pi\right], \tag{5}$$

where n represents the phase-shift index $n = 1, 2, \ldots, N$.

The values of phase $\phi(x,y)$ can be calculated by

$$\phi(x,y) = -\tan^{-1}\left[\frac{\sum_{n=1}^{N} I_n(x,y)\sin\left(\frac{n-1}{N}2\pi\right)}{\sum_{n=1}^{N} I_n(x,y)\cos\left(\frac{n-1}{N}2\pi\right)}\right]. \tag{6}$$

Since there are three unknowns, $I_0(x,y)$, $M(x,y)$ and $\phi(x,y)$, in Equation 5, at least three images, $I_1(x,y)$, $I_2(x,y)$ and $I_3(x,y)$, should be used to enable the calculation of $\phi(x,y)$.

In Equation 5, we considered the intensity of the sinusoidal fringes. However, the nonlinearity of the luminance caused by the gamma effect of the digital camera and projector introduces significant harmonics that lead to errors in the phase determination [48]-[51].

Considering the harmonics, and indicating with H the highest significant harmonic order of the captured fringes, Equation 5 can be rewritten as [52]

$$I_n(x,y) = I_0(x,y) + \sum_{k=1}^{H} M_k(x,y)\cos\left[k\left(\phi(x,y) + \frac{n-1}{N}2\pi\right)\right] \tag{7}$$

Equation (7) involves $(H+2)$ unknowns: $I_0(x,y)$, $M_1(x,y)$, ... , $M_k(x,y)$, ... , $M_H(x,y)$ and $\phi(x,y)$; consequently, $N = H+2$ phase-shifted fringe patterns are required to solve these unknowns.

Therefore, if we consider a set of $N = H+2$ uniform phase-shifted sinusoidal fringe patterns, the values of the phase can be retrieved by means of

$$\phi^w(x,y) = -\tan^{-1}\left[\frac{\sum_{n=1}^{H+2} I_n(x,y)\sin\left(\frac{n-1}{H+2}2\pi\right)}{\sum_{n=1}^{H+2} I_n(x,y)\cos\left(\frac{n-1}{H+2}2\pi\right)}\right]. \tag{8}$$

Equation 8 indicates that an $H+2$ uniform phase-shifted scheme can be employed to retrieve the phase accurately from the fringe patterns with nonlinear harmonics up to the Hth order.

Generally, the highest significant harmonic order, in practice, is below eight.

Commonly, phase $\phi(x,y)$ can be distributed over an interval greater than 2π. Unfortunately, the arctan function, using the numerator and denominator signs, returns values of $\phi^w(x,y)$ only in the range from $-\pi$ to $+\pi$. In other words, the phase is rolled up in a 2π interval. Superscript w denotes a wrapped phase value.

To recover the correct phase value, it is necessary to use an unwrapping phase procedure. This results in an unwrapped phase map, which is given by Equation (9):

$$\phi^w(x,y) = \phi(x,y) + 2\pi \cdot q(x,y)\,, \tag{9}$$

where $q(x,y)$, the number of turns, is an integer that may be positive or negative.

3. PHASE UNWRAPPING

Phase unwrapping is the restoration of the original phase values of an image, given the observed wrapped values. While, theoretically, this problem can be easily solved, this is not the case for 'experimental' wrapped phases. Indeed, when a complex object is measured, abrupt and irregular changes in the measured surface may result in local shadows.

With the use of computer-generated fringe patterns, however, the phase in the projected fringe pattern can be easily programmed. Therefore, temporal phase unwrapping techniques can be used for recovered phase maps [53]-[55]. The temporal phase combines phase shifting with a change in fringe pitch (change in wavelength or distance between fringes). The strength of the method is that the problem with phase rolling never occurs and that it results in an absolute phase measurement.

Temporal phase unwrapping offers several potential advantages over the spatial method [56]:

- errors do not propagate to the whole phase map
- fringe order errors can be easily detected and filtered out 'a posteriori' since they are multiples of 2π
- it does not require user intervention to indicate specimen edges or to provide the phase value at a particular point
- it is very fast and does not require additional memory
- the implementation is extremely simple.

However, temporal phase unwrapping has the disadvantage of working well only with the hypothesis of static objects. In other words, throughout the process, it is critical that the measured quantities be of temporal invariance.

The idea of temporal phase unwrapping is to use a sequence of fringe maps with a change in fringe pitch (see Figure 5). In other words, frequency repeats single phase shifting M times with periods of the fringe at $d_1, d_2, \dots, d_t, \dots, d_M$.

In the fringe pattern, the relative phases are $\phi(x,y;1), \phi(x,y;2), \dots, \phi(x,y;t), \dots, \phi(x,y;M)$.

For subsequent time values ($t = 1, 2, 4, \dots, M$), the number of fringes is also set equal to t so that the phase range increases to $(-t \cdot \pi, +t \cdot n)$.

There is a linear relationship between the phase and the number of the projected fringe. If one phase jump is projected, we have one fringe of wrapped phase map; when projecting two fringes, the wrapped phase map contains exactly two phase jumps. In temporal phase unwrapping, the phase difference is calculated from successive frames. This technique is inherently robust.

Wrapped phase measurements for each used fringe period are acquired sequentially in time.

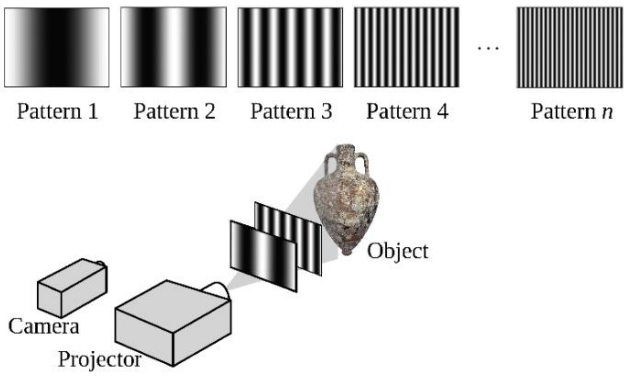

Figure 5. Sequence of fringe maps projected onto an object surface. For each t value, $H + 2$ phase-stepped images are acquired.

By means of Equation 8, for each t, we obtain a wrapped phase.

Initially, a single fringe ($t = 1$) is projected so that the fringe phase range is only from $-\pi$ to $+\pi$.

Therefore,

$$\phi^u(x,y;1) = \phi^w(x,y;1)\,. \tag{10}$$

For subsequent time values ($t = 2, 4, \dots, M$), the number of fringes is also set equal to t so that the phase range increases to $(-t \cdot \pi, +t \cdot n)$. With this procedure, for each t value, $H + 2$ phase-stepped images are acquired.

The unwrapped phase distributions of the higher frequency fringes can be readily calculated without a general phase unwrapping. The algorithm can be expressed as follows [55], [56]:

$$\phi^u(x,y;t) = \phi^w(x,y;t) + NINT\left[\frac{\phi^u(x,y;t-1) - \phi^w(x,y;t)}{\pi}\right] \cdot 2\pi\,, \tag{11}$$

where $NINT(.)$ denotes rounding to the nearest integer.
Using an iterative process, the unwrapped phase can be computed by summing the wrapped phase difference between the successive phase maps.

Figure 6 shows an example of a sequence of fringe maps achieved with our system.

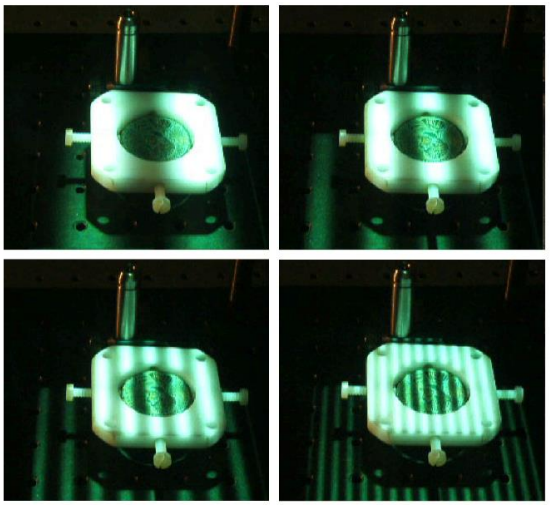

Figure 6. Example of fringe maps used in our system.

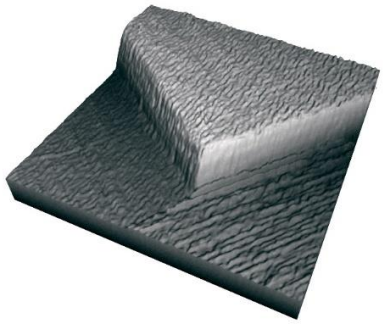

Figure 7. Three-dimensional reconstruction of specimen with 50 µm calibrated steps.

In the presence of noise, as generally occurs, a better approach to the estimation of the unwrapped phase is a fitting, in the least-squares sense of the line defined by Equation 9, to the experimental data [57]:

$$\hat{\phi}^u(x,y) = \frac{\sum_{t=1}^{M}[t \cdot \phi_t^u(x,y;t)]}{\sum_{t=1}^{M} t^2}. \quad (12)$$

Since the algorithm involves only one single governing equation, it is very simple and easy to use.

4. EXPERIMENTAL RESULTS AND DISCUSSION

First, some validation experiments were conducted. Figure 7 shows the recovered 2.5D plot from a metallic specimen (2.5 cm × 2.5 cm) with a step of 50 µm in height. The specimen was realised by means of a grinding machine. A comparison between the conventional direct contact measurement and the optical results shows that the maximum discrepancy is about 2 µm.

Subsequently, we performed a test on a telephone token. Figure 8 shows the recovered 2.5D plot of an Italian telephone token, in use in Italy from 1959 until 2001.

Dimensional measurements of the throat profile were obtained to check the quality of the 2.5D reconstruction. An example of a profile is shown in Figure 9.

Again, the discrepancies between the optical measurement and direct contact measurement are less than 2 µm.

Considering the characteristics of our system, it is well suited to 2.5D coin reconstruction. In general, coins can be analysed in two and three dimensions. The advantage of 3D coin data is that it allows a more detailed and reliable analysis due to an exact description of the coin's surface, which is a great benefit for any automated classification or recognition task [59]-[61].

To check the usability of the instrumentation for the 3D survey, we surveyed the surface topography of some coins.

We initially acquired the relief of an old Italian 10 Lire coin used before 2000. Figure 10 shows the recovered 2.5D plot; it

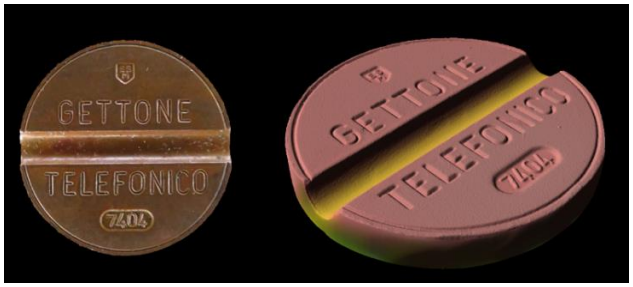

Figure 8. Recovered 2.5D Italian telephone token (diameter ø = 24 mm).

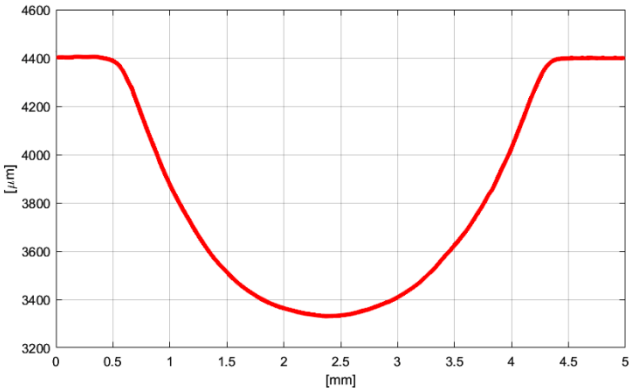

Figure 9. Depth profile plot of the telephone token throat.

can be noted that the three-dimensional details are correctly reconstructed.

Finally, the surface topography of a New Zealand one-cent piece is shown in Figure 11. On the reverse of the coin, a fern leaf is represented. In the 2.5D plot, all the details are correctly reconstructed.

5. PIPELINE FOR 3D COLOUR MODEL

For a correct and accurate acquisition of the surface, it is essential that the colour characteristics are also acquired.

In a typical 3D data elaboration pipeline, to obtain a complete 3D model of the acquired object from the raw data, the following steps should be followed:

- Acquisition of 2D colour information [62], [63].
- 3D geometric data acquisition.
- Data integration.
- Model conversion.

Figure 10. Recovered 3D plot of a coin: '10 Italian lire' (ear of corn; coin diameter ø = 23.3 mm).

Figure 11. Recovered 2.5D plot of a coin: 1 Cent, New Zealand (standard circulation 1967–1985; 'fern leaf' on the reverse; coin diameter ø = 17.4 mm).

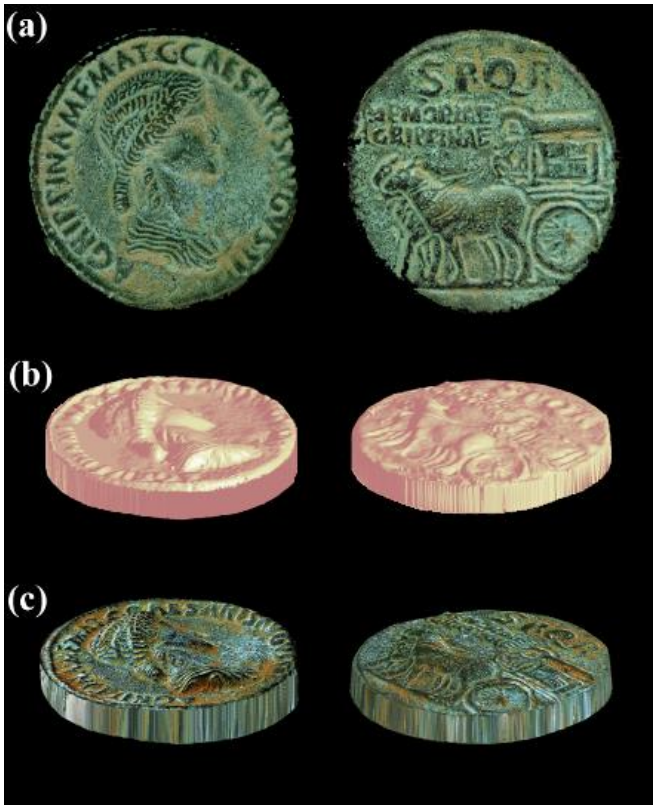

Figure 12. Ancient Roman coin (A.D. 37–41). (a) Photograph of the coin: obverse and reverse; (b) Shaded rendering of the coin geometry; (c) Rendering of the coin shape and colour model (diameter ø = 33 mm).

To test the usability of the proposed technique in the construction of a virtual gallery of ancient artifacts, we have digitised some ancient Roman coins.

Figure 12 shows the data-processing pipeline steps used to obtain a complete 3D model of a Roman sestertius of Agrippina Senior, who was born in 15 B.C. and died in exile in A.D. 33. This commemorative coin, bearing her name and portrait, was struck by her son, the Emperor Caligula (A.D. 37–41).

Figure 12(a) shows the colour photos of the coins (obverse and reverse), Figure 12(b) provides the shared view of the geometry with surface details and Figure 12(c) depicts the colour rendering of the coin.

It is important to note that our system is only capable of a correct 2.5D reconstruction. Therefore, the reverse side of the coin has not been reconstructed.

6. CONCLUSIONS

Projected fringes for the measurement of surface profiles are extensively used in 2.5D optical metrology. However, low-cost, commercially available projectors are susceptible to gamma non-linearity and a lack of depth of field, which distorts the fringe patterns and introduces significant errors in the phase measurements. In this work, we have presented a simple optical method that can be applied to the measurement of micro-surface profiles. In the proposed setup, the number of phase shifts applied in the projected grating can be changed via the user interface, depending on the accuracy required.

The proposed device has the potential of the traditional fringe projection technique but with more versatility, offering the freedom to choose and control the fringe period. Experiments using real samples have shown that the 2.5D profiling measured using the proposed system is efficient and effective. Furthermore, the method relies on very simple and cheap equipment.

The proposed system uses only consumer-available technology (a video projector and a digital camera) and can be achieved for less than $ 1,000.

In other words, for less than $ 1,000, it is possible to achieve a system with precision and accuracy that is comparable to much more complex and expensive systems (> $ 5,000).

REFERENCES

[1] G. Sansoni, M. Trebeschi, F. Docchio, State-of-the-art and applications of 3D imaging sensors in industry, cultural heritage, medicine, and criminal investigation, Sensors 9 (2009), pp. 568-601.
DOI: 10.3390/s90100568

[2] G. Sansoni, F. Docchio, 3-D optical measurements in the field of cultural heritage: the case of the Vittoria Alata of Brescia, IEEE Trans. Instrum. Meas. 54 (2005), pp. 359-368.
DOI: 10.1109/TIM.2004.838915

[3] F. Remondino, Heritage recording and 3D modeling with photogrammetry and 3D scanning, Remote Sensing 3 (2011), pp. 1104-1138.
DOI: 10.3390/rs3061104

[4] J. Von Schwerin, H. Richards-Rissetto, F. Remondino, G. Agugiaro, G. Girardi, The MayaArch3D project: a 3D WebGIS for analyzing ancient architecture and landscapes, Literary and Linguistic Computing 28 (2013), pp. 736-753.
DOI: 10.1093/llc/fqt059

[5] S.G. Barsanti, F. Remondino, B.J. Fenández-Palacios, D. Visintini, Critical factors and guidelines for 3D surveying and modelling in cultural heritage, International Journal of Heritage in the Digital Era 3 (2014), pp. 141-158.
DOI: 10.1260/2047-4970.3.1.141

[6] G. Palma, P., Pingi, E. Siotto, R. Bellucci, G., Guidi, R. Scopigno, Deformation analysis of Leonardo da Vinci's "Adorazione dei Magi" through temporal unrelated 3D digitization, Journal of Cultural Heritage 38 (2019), pp. 174-185.
DOI: 10.1016/j.culher.2018.11.001

[7] G. Schirripa Spagnolo, R. Majo, M. Carli, A. Neri, 3D scanner and virtual gallery of small cultural heritage objects, Proc. SPIE 5302, Three-Dimensional Image Capture and Applications VI, San Jose, USA, 16 April 2004, pp. 148-155.
DOI: 10.1117/12.527983

[8] J.A. Rayas, M. León-Rodríguez, A. Martínez-García, R. Cordero, Gates' interferometer as fringe projection system for recovering 3D shapes, Proc. of the 5th International Symposium on Experimental Mechanics and 9th Symposium on Optics in Industry (ISEM-SOI), Guanajuato, Mexico, 17 - 21 August 2015, pp. 153-158.
DOI: 10.1007/978-3-319-28513-9_21

[9] I. Stancic, J. Music, V. Zanchi, Improved structured light 3D scanner with application to anthropometric parameter estimation, Measurement 46 (2013), pp. 716-726.
DOI: 10.1016/j.measurement.2012.09.010

[10] B. Trifkovic, I. Budak, A. Todorovic, D. Vukelic, V. Lazic, T. Puskar, Comparative analysis on measuring performances of dental intraoral and extraoral optical 3D digitization systems, Measurement 47 (2014), pp. 45-53.
DOI: 10.1016/j.measurement.2013.08.051

[11] G. Schirripa Spagnolo, Potentiality of 3D laser profilometry to determine the sequence of homogenous crossing lines on questioned documents, Forensic Sci Int. 164 (2006), pp. 102-199.
DOI: 10.1016/j.forsciint.2005.12.004

[12] G. Schirripa Spagnolo, L. Cozzella, C. Simonetti, Linear conoscopic holography as aid for forensic handwriting expert, Optik 124 (2013), pp. 2155-2160.
DOI: 10.1016/j.ijleo.2012.06.097

[13] D. Raneri, Enhancing forensic investigation through the use of modern three-dimensional (3D) imaging technologies for crime scene reconstruction, Australian Journal of Forensic Sciences 50 (2018), pp. 697-707.
DOI: 10.1080/00450618.2018.1424245

[14] D. Ott, R. Thompson, J. Song, Applying 3D measurements and computer matching algorithms to two firearm examination proficiency tests, Forensic Science International 271 (2017), pp. 98-106.
DOI: 10.1016/j.forsciint.2016.12.014.

[15] D. Smeets, P. Claes, D. Vandermeulen, J.G. Clement, Objective 3D face recognition: Evolution, approaches and challenges, Forensic Science International 201 (2010), pp. 125-132.
DOI: 10.1016/j.forsciint.2010.03.023

[16] G. Schirripa Spagnolo, L. Cozzella, C. Simonetti, IR fringe projection for 3D face recognition, Int. Conf. On Advanced Phase Measurement Methods In Optics And Imaging, Monte Verita (Ascona), Italy, 16-21 May 2010, AIP Conference Proceedings 1236 383 (2010)
DOI: 10.1063/1.3426146

[17] G. Sansoni, P. Bellandi, F. Docchio, Design and development of a 3D system for the measurement of tube eccentricity, Meas. Sci. Technol. 22 (2011) 075302.
DOI: 10.1088/0957-0233/22/7/075302

[18] G. Sansoni, P. Bellandia, F. Leonia, F. Docchio, Optoranger: A 3D pattern matching method for bin picking applications, Opt Lasers Eng 54 (2014), pp. 222-231.
DOI: 10.1016/j.optlaseng.2013.07.014

[19] G. Schirripa Spagnolo, L. Cozzella, F. Leccese, Viability of an optoelectronic system for real time roughness measurement, Measurement 58 (2014), pp. 537-543.
DOI: 10.1016/j.measurement.2014.09.018

[20] M. Hawryluk, J. Ziemba, Application of the 3D reverse scanning method in the analysis of tool wear and forging defects, Measurement 128 (2018), pp. 204-213.
DOI: 10.1016/j.measurement.2018.06.037

[21] M. Massot-Campos, G. Oliver-Codina, Optical sensors and methods for underwater 3D reconstruction, Sensors 15 (2015), pp. 31525-31557.
DOI: 10.3390/s151229864

[22] G. Schirripa Spagnolo, L. Cozzella, F. Leccese, Underwater optical wireless communications: overview, Sensors 20 (2020), p. 14.
DOI: 10.3390/s20082261

[23] S. Zhang, High-speed 3D shape measurement with structured light methods: a review, Opt. Lasers Eng. 106 (2018), pp. 119-131.
DOI: 10.1016/j.optlaseng.2018.02.017

[24] J. Salvi, S. Fernandez, T. Pribanic, X. Llado, A state of the art in structured light patterns for surface profilometry, Pattern Recognition 43 (2010), pp. 2666-2680,
DOI: 10.1016/j.patcog.2010.03.004

[25] S. S. Gorthi, P. Rastogi, Fringe projection techniques: whither we are? Optics and Lasers in Engineering 48 (2010), pp. 133-140.
DOI: 10.1016/j.optlaseng.2009.09.001

[26] C. S. Lin, T. L. Horng, J. H. Chen, K. H. Chen, J. J. Wu, C. Y. Chen, S. H. Ma, Mechanical properties measurement of polymer films by bulge test and fringe projection, Advances in Materials Science and Engineering 2014 (2014) 170279.
DOI: 10.1155/2014/170279

[27] G. Schirripa Spagnolo, L. Cozzella, F. Leccese, Projected fringes profilometry for cultural heritage studies, Proc. of the IMEKO TC-4 International Conference on Metrology for Archaeology and Cultural Heritage, Florence, Italy, 4 – 6 December 2019, pp. 435-438. Online [Accessed 29 April 2020]
https://www.imeko.org/publications/tc4-Archaeo-2019/IMEKO-TC4-METROARCHAEO-2019-85.pdf

[28] S. Zhang, Handbook of 3D Machine Vision: Optical Metrology and Imaging, CRC Press, Boca Raton, 2013.
DOI: 10.1201/b13856

[29] D. Li, C. Liu, J. Tian, Telecentric 3D profilometry based on phase-shifting fringe projection, Opt. Express 22 (2014), pp. 31826-31835.
DOI: 10.1364/OE.22.031826

[30] F. Chen, G.M. Brown, M. Song, Overview of three-dimensional shape measurement using optical methods, Opt. Eng. 39 (2000), pp.10-22.
DOI: 10.1117/1.602438

[31] Z. Zhang, D. Zhang, X. Peng, Performance analysis of a 3D full-field sensor based on fringe projection, Opt. Lasers Eng. 42 (2004), pp. 341-353.
DOI: 10.1016/j.optlaseng.2003.11.004

[32] T. Yoshizawa, Handbook of Optical Metrology Principles and Applications (Second Edition), CRC Press, Boca Raton, 2009.
DOI: 10.1201/b18328

[33] Y. Wen, S. Li, H. Cheng, X. Su, Q. Zhang, Universal calculation formula and calibration method in Fourier transform profilometry, Appl. Opt. 49 (2010), pp. 6563-6569.
DOI: 10.1364/AO.49.006563

[34] Y. Wen, H. Cheng, Y. Gao, H. Zhang, Y. Feng, B. Pan, Least-squares calibration method based on a universal phase and height mapping formula in Fourier transform profilometry, Measurement Science and Technology 22 (2011) 105303.
DOI: 10.1088/0957-0233/22/10/105303

[35] W. Li, X. Su, L. Su, A practical coordinate mapping method for phase-measuring profilometry, Proc. SPIE Vol. 3558, Automated Optical Inspection for Industry: Theory, Technology, and Applications II, Photonics China '98, Beijing, China, 10 August 1998, pp. 125-130.
DOI: 10.1117/12.318369

[36] S. Ma, C. Quan, R. Zhu, C.J. Tay, Investigation of phase error correction for digital sinusoidal phase-shifting fringe projection profilometry, Optics and Lasers in Engineering 50 (2012), pp. 1107-1118.
DOI: 10.1016/j.optlaseng.2012.01.021

[37] L.C. Chen, C.C. Liao, Calibration of 3D surface profilometry using digital fringe projection, Meas. Sci. Technol. 16 (2005), pp. 1554-1566.
DOI: 10.1088/0957-0233/16/8/003

[38] X. Zhang, Y. Lin, M. Zhao, Calibration of a fringe projection profilometry system using virtual phase calibrating model planes, J. Opt. A: Pure Appl. Opt. 7 (2005), pp. 192-197.
DOI: 10.1088/1464-4258/7/4/007

[39] P.J. Tavares, M.A. Vaz, Linear calibration procedure for the phase-to-height relationship in phase measurement profilometry, Opt. Commun. 274 (2007) pp. 307-314.
DOI: 10.1016/j.optcom.2007.02.038

[40] M. Takeda, K. Mutoh, Fourier transform profilometry for the automatic measurement of 3-D object shaped, Appl. Opt. 22 (1983), pp. 3977-3982.
DOI: 10.1364/AO.22.003977

[41] E. Zappa, G. Busca, Static and dynamic features of Fourier transform profilometry: a review, Optics and Lasers in Engineering 50 (2012), pp. 1140-1151.
DOI: 10.1016/j.optlaseng.2012.03.008

[42] G. Schirripa Spagnolo, L. Cozzella, F. Leccese, Phase correlation functions: FFT vs. FHT, ACTA IMEKO 8 (2019), pp. 87-92.
DOI: 10.21014/acta_imeko.v8i1.604

[43] K. Creath, Phase-measurement interferometry techniques, in: Progress in Optics. E. Wolf (editor), Volume 26, 1988, pp. 349-393.
DOI: 10.1016/S0079-6638(08)70178-1

[44] C. Zuo, S. Feng, L. Huang, T. Tao, W. Yin, Q. Chen, Phase shifting algorithms for fringe projection profilometry: a review, Optics and Lasers in Engineering 109 (2018) pp. 23-59.
DOI: 10.1016/j.optlaseng.2018.04.019

[45] H. Zhu, S. Xing, H. Guo, Efficient depth recovering method free from projector errors by use of pixel cross-ratio invariance in fringe projection profilometry, Applied Optics 59 (2020) pp. 1145-1155.
DOI: 10.1364/AO.383204

[46] T. W. Hui, G. K. H. Pang, 3D profile reconstruction of solder paste based on phase shift profilometry, Proc. of the 5th IEEE International Conference on Industrial Informatics, Vienna, Austria, 23 – 27 June 2007, pp. 165-170. DOI: 10.1109/INDIN.2007.4384750

[47] P. S. Huang, Q. Hu, F. P. Chiang, Error compensation for a 3D shape measurement system, Opt. Eng. 42 (2003) pp. 482-486. DOI: 10.1117/1.1531636

[48] H. Lei, P. S. K. Chua, A. Asundi, Least-squares calibration method for fringe projection profilometry considering camera lens distortion, Appl. Opt. 49 (2010) pp. 1539-1548. DOI: 10.1364/AO.49.001539

[49] B. Pan, Q. Kemao, L. Huang, A. Asundi, Phase error analysis and compensation for nonsinusoidal waveforms in phase-shifting digital fringe projection profilometry, Optics Letters 34 (2009) pp. 416-418. DOI: 10.1364/OL.34.000416

[50] K. Liu, Y. Wang, D. L. Lau, Q. Hao, L.G. Hassebrook, Gamma model and its analysis for phase measuring profilometry, Journal of the Optical Society of America A (2010) pp. 553-562. DOI: 10.1364/JOSAA.27.000553

[51] T. Hoang, B. Pan, D. Nguyen, Z. Wang, Generic gamma correction for accuracy enhancement in fringe-projection profilometry, Optics Letters 35 (2010) pp. 1992-1994. DOI: 10.1364/OL.35.001992

[52] Y. Surrel, Design of algorithms for phase measurements by the use of phase stepping, Applied Optics 35 (1996) pp. 51-60. DOI: 10.1364/AO.35.000051

[53] H. O. Saldner, J. M. Huntley, Temporal phase unwrapping: application to surface profiling of discontinuous objects, Appl. Opt. 36 (1997) pp. 2270-2275. DOI: 10.1364/AO.36.002770

[54] C. Zuo, L. Huang, M. Zhang, Q. Chen, A. Asundi, Temporal phase unwrapping algorithms for fringe projection profilometry: a comparative review, Opt Lasers Eng 85 (2016) pp. 84-103. DOI: 10.1016/j.optlaseng.2016.04.022

[55] S. Xing, H. Guo, Temporal phase unwrapping for fringe projection profilometry aided by recursion of Chebyshev polynomials, Appl. Opt. 56 (2017) pp. 1591-1602. DOI: 10.1364/AO.56.001591

[56] A. Baldi, F. Bertolino, F. Ginesu, A temporal phase unwrapping algorithm for photoelastic stress analysis, Optics and Lasers in Engineering 45 (2007) pp. 612-617. DOI: 10.1016/j.optlaseng.2006.08.006

[57] H. O. Saldner, J. M. Huntley, Shape measurement of discontinuous objects using projected fringes and temporal phase unwrapping, Proc. of the International Conference on Recent Advances in 3-D Digital Imaging and Modeling (Cat. No.97TB100134), Ottawa, Canada, 12-15 May 1997, pp. 44-50. DOI: 10.1109/IM.1997.603847

[58] Y. Fu, W. Wang, H. Xiao, Three-dimensional profile measurement based on modified temporal phase unwrapping algorithm, Optik 124 (2013) pp. 557-560. DOI: 10.1016/j.ijleo.2011.12.022

[59] M. Kampel, S. Zambanini, M. Schlapke, B. Breuckmann, Highly detailed 3D scanning of ancient coins, Proc. of the 22nd CIPA Symposium, Kyoto, Japan, 11 – 15 October 2009. Online [Accessed 29 April 2020] https://www.cipaheritagedocumentation.org/wp-content/uploads/2018/12/Kampel-e.a.-Highly-Detailed-3D-Scanning-of-Ancient-Coins.pdf

[60] L. MacDonald, V. Moitinho de Almeida, M. Hessa, Three-dimensional reconstruction of Roman coins from photometric image sets, Journal of Electronic Imaging 26 (2017) 011017. DOI: 10.1117/1.JEI.26.1.011017

[61] S. Zambanini, M. Schlapke, M. Hödlmoser, M. Kampel, 3D acquisition of historical coins and its application area in numismatics, Proc. SPIE 7531, Computer Vision and Image Analysis of Art, San Jose, California, United States, 16 February 2010, 753108. DOI: 10.1117/12.840203

[62] K. E. Torrance, E. M. Sparrow, Theory for off-specular reflection from roughened surfaces, J.OSA 57 (1967) pp. 1105-1114. DOI: 10.1364/JOSA.57.001105

[63] G. Schirripa Spagnolo, B. Calabrese, G. Ferrari, Color separation to facilitate handwriting examination, Proc. of the 5th International Symposium on Communications Control and Signal Processing, ISCCSP 2012, Rome, Italy, 2-4 May 2012, 4 pp. DOI: 10.1109/ISCCSP.2012.6217832